Unclassified

SECURITY CLASSIFICATION OF THIS PAGE

MENTATION PAGE

Form Approved
OMB No. 0704-0188

AD-A213 251

1a.

1b. RESTRICTIVE MARKINGS

2a.

3. DISTRIBUTION / AVAILABILITY OF REPORT
Approved for public release; distribution unlimited

2b. DECLASSIFICATION / DOWNGRADING SCHEDULE

4. PERFORMING ORGANIZATION REPORT NUMBER(S)
N00014-85-K-0646 (Final Report)

5. MONITORING ORGANIZATION REPORT NUMBER(S)

6a. NAME OF PERFORMING ORGANIZATION
Aeronautics Department
California Inst. of Technology

6b. OFFICE SYMBOL (If applicable)

7a. NAME OF MONITORING ORGANIZATION

DTIC ELECTE OCT 10 1989 S D

6c. ADDRESS (City, State, and ZIP Code)
Pasadena, California 91125

7b. ADDRESS (City, State, and ZIP Code)

8a. NAME OF FUNDING / SPONSORING ORGANIZATION
Office of Naval Research

8b. OFFICE SYMBOL (If applicable)

9. PROCUREMENT INSTRUMENT IDENTIFICATION NUMBER
N00014-85-K-0646

8c. ADDRESS (City, State, and ZIP Code)
800 N. Quincy Street
Arlington, Virginia 22217-5000

10. SOURCE OF FUNDING NUMBERS

PROGRAM ELEMENT NO.	PROJECT NO.	TASK NO.	WORK UNIT ACCESSION NO.
			4328-434

11. TITLE (Include Security Classification)
Structure of the Compressible Turbulent Shear Layer (unclassified)

12. PERSONAL AUTHOR(S)
Dimitri Papamoschou

13a. TYPE OF REPORT	13b. TIME COVERED	14. DATE OF REPORT (Year, Month, Day)	15. PAGE COUNT
Final Report	FROM 1/7/85 TO 10/31/88	89/9/26	12

16. SUPPLEMENTARY NOTATION
AIAA Paper 89-0126, 1989
Presented at the AIAA 27th Aerospace Sciences Meeting, January 1989, Reno, Nevada.

17. COSATI CODES		
FIELD	GROUP	SUB-GROUP

18. SUBJECT TERMS (Continue on reverse if necessary and identify by block number)
turbulent flow;
supersonic flow.

19. ABSTRACT (Continue on reverse if necessary and identify by block number)

The large-scale structure of the turbulent compressible shear layer is investigated in a two-stream supersonic wind tunnel through a series of experiments. Double-exposure schlieren photography reveals that the two convective Mach numbers, corresponding to each side of the shear layer, are very different, one sonic or supersonic and the other low subsonic. This contradicts the current isentropic model of the structure which predicts them to be equal or very close. It is shown that addition of shock-wave effects to that model allows for the asymmetric trends observed in the experiments. An inclined view of the flow provides sketchy information about the spanwise orientation of the large-scale structure and does not reveal any pronounced obliquity. Attempts to enhance mixing by modifying the trailing edge were unsuccessful.

20. DISTRIBUTION / AVAILABILITY OF ABSTRACT
☒ UNCLASSIFIED/UNLIMITED ☐ SAME AS RPT. ☐ DTIC USERS

21. ABSTRACT SECURITY CLASSIFICATION
Unclassified

22a. NAME OF RESPONSIBLE INDIVIDUAL

22b. TELEPHONE (Include Area Code)

22c. OFFICE SYMBOL

DD Form 1473, JUN 86 *Previous editions are obsolete.*

SECURITY CLASSIFICATION OF THIS PAGE
Unclassified

AIAA '89

AIAA-89-0126

Structure of the Compressible Turbulent Shear Layer

D. Papamoschou
California Institute of Technology
Pasadena, CA

27th Aerospace Sciences Meeting
January 9-12, 1989/Reno, Nevada

Structure of the Compressible Turbulent Shear Layer

Dimitri Papamoschou *
California Institute of Technology, Pasadena, California

Abstract

The large-scale structure of the turbulent compressible shear layer is investigated in a two-stream supersonic wind tunnel through a series of experiments. Double-exposure schlieren photography reveals that the two convective Mach numbers, corresponding to each side of the shear layer, are very different, one sonic or supersonic and the other low subsonic. This contradicts the current isentropic model of the structure which predicts them to be equal or very close. It is shown that addition of shock-wave effects to that model allows for the asymmetric trends observed in the experiments. An inclined view of the flow provides sketchy information about the spanwise orientation of the large-scale structure and does not reveal any pronounced obliquity. Attempts to enhance mixing by modifying the trailing edge were unsuccessful.

Nonmenclature

a	speed of sound
M	free stream Mach number
M_c	convective Mach numer (unspecified side)
U	free stream velocity
U_c	convective velocity
β	obliquity angle
γ	specific-heat ratio
δ'	growth rate
θ	boundary-layer momentum thickness
ρ	density

Subscripts:

1	high-speed stream
2	low-speed stream

*Research Fellow, Member AIAA
Now Assistant Professor, U. C. Irvine

Introduction

It is a widely-accepted premise that shear-layer entrainment and mixing are governed by the instability of the turbulent large-scale structure. The visualization of such structures in the compressible case led Papamoschou and Roshko[1,2] to characterize the compressibility of the flow in a frame of reference in which the structure is stationary. Given the flow conditions depicted in Fig. 1, this was done by defining the *convective Mach numbers* as follows:

$$M_{c_1} = \frac{U_1 - U_c}{a_1} \qquad M_{c_2} = \frac{U_c - U_2}{a_2} \tag{1}$$

where U_c is the convective velocity of the structure, assumed to be constant.

The relation between M_{c_1} and M_{c_2} was obtained by requiring that the total pressures of the two streams in the convective frame be equal. This stems from a well-known argument, used primarily with subsonic flows, that there exists a stagnation point between two structures that must be stable, thus the pressures at that point must balance (Fig. 2). It has been proposed explicitly or implicitly by a variety of investigators (Flügel[3], Brown[4], Coles[5], Dimotakis[6]).

The above argument was first extended to compressible flow by Bogdanoff[7]. This extension, used subsequently by Papamoschou and Roshko, assumes that the flow comes to rest at the stagnation point *isentropically*, hence with no shock-wave losses, even for supersonic convective Mach numbers. For streams with equal specific-heat ratios ($\gamma_1 = \gamma_2$) one simply gets

$$M_{c_1} = M_{c_2} = \frac{\Delta U}{a_1 + a_2} \tag{2}$$

where $\Delta U \equiv U_1 - U_2$. For the cases where $\gamma_1 \neq \gamma_2$, M_{c_1} and M_{c_2} are slightly unequal but (2) is still a good

approximation. Using (1) and (2), an expression for U_c is obtained:

$$\frac{U_c - U_2}{U_1 - U_2} = \frac{1}{1 + \sqrt{\frac{\rho_2}{\rho_1}}} \tag{3}$$

which is identical to that obtained by the subsonic argument. The experiments of Brown and Roshko[8] demonstrated the validity of (3) for incompressible, variable-density flow.

Since M_{c_1} and M_{c_2} are theoretically equal or very close, Papamoschou and Roshko chose M_{c_1} as a compressibility-effect paramater against which the shear-layer growth rate was correlated. Their result is shown on Fig. 3, where the growth rate, δ', is normalized by its incompressible value, δ'_0. The fact that all the experimental points, corresponding to a large range of free stream conditions, collapsed roughly onto one curve demonstrated the applicability of of the convective Mach number as a measure of shear-flow compressibility.

Nevertheless, questions remained as to the accuracy of (2) and (3) when shock waves form on the structure, since their effects are not addressed by the above model. There is little doubt that shock waves will occur as the convective Mach number exceeds some critical value. This is the basic motivation for the work described here, in which the convective Mach numbers were measured experimentally. Additionally, experiments related to the spanwise organization of the large-scale structure and to mixing enhancement were conducted and are described in later sections of this paper.

Experiment

Experiments were conducted in the GALCIT 25mm × 57mm × 200mm supersonic shear layer facility, extensively described in previous reports[1,2,9]. Typical flow static pressures were 0.1 atm., with the resulting unit Reynolds numbers of the order of 10^4 per mm. In the region of the measurements, x/θ_1 exceeded 1000, where θ_1 is the trailing-edge momentum tickness for the high-speed stream. The flow is thus believed to be fully-developed turbulent.

Convective velocity measurements were taken by means of a two-spark variant of the schlieren method, developed by the author. Its operating principle is illustrated on Fig. 4. A detailed description of the system will be provided in a different publication[10]. It retains the basic elements of a schlieren system, only now there are two slightly off-axis beams produced by two different spark gaps. By means of the prism shown on the schematic, the source focal points of the two beams coincide at the single knife edge and two distinct images appear on the film. The exposure time of each image is 20 ns, short enough to capture the details of the flow.

The time interval between spark firings (and hence betwen images), Δt, is controllable. During that time interval, a large-scale-structure feature moves a distance Δx. The convective velocity is simply $U_c = \Delta x/\Delta t$. The convective Mach numbers are then obtained from (1).

The measurement error for U_c is roughly ±5%, based on the uncertainty in locating a given feature from one exposure to the next. For M_c, this translates to an error of the order of $\pm 5\%/M_c$. Clearly, for M_c close to zero, this is a substantial error. But for M_c of the order of one, the error is similar to that for U_c.

Fig. 5 shows actual measurements of U_c from two-spark schlieren photos for three of the ten Mach number-gas combinations explored in this study. Arrows indicate the structure features on which the measurements are based. These photos were taken with the knife edge parallel to the flow direction and span a distance from 50mm to 140mm from the trailing edge. Other knife edge orientations, such as 45-deg. and perpendicular, were also tried and did not produce any difference in the U_c measurements (see Fig. 14). For all cases, U_c was found to be independent of streamwise position. The standard deviation of the measurements is within the experimental error margin.

Results

The table that follows summarizes the experimental conditions and convective Mach number measurements. Ten cases of different Mach number-gas combinations are listed. For brevity and ease of reference, each case is assigned a code name consisiting of the gases and Mach numbers. Letters represent the gases: A for argon (γ=1.67), H for helium (γ=1.67), N for nitrogen (γ=1.4), and S for sulfur hexafluoride (SF_6, γ=1.09). Numbers represent the Mach numbers times 10. For example, A32S03 is the case with argon

at M_1=3.2 and SF_6 at M_2=0.3. The faster stream is placed first in the name.

The cases are listed in order of increasing $\frac{\Delta U}{a_1+a_2}$. As noted previously, this parameter is very close or equal to the theoretical M_{c_1} and M_{c_2}, so it replaces them in the table. The last column contains the number of data points (N) reflected in each measurement.

CASE	$\frac{U_2}{U_1}$	$\frac{\rho_2}{\rho_1}$	$\frac{\Delta U}{a_1+a_2}$	M_{c_1}	M_{c_2}	N
A32N16	0.94	0.24	0.07	0.07	0.07	5
N31N17	0.75	0.54	0.33	0.29	0.36	6
N28A26	0.75	1.8	0.38	0.48	0.26	8
H17N28	0.50	9.2	0.65	0.83	0.10	10
A32A02	0.13	0.23	0.90	0.39	1.14	8
S27S03	0.13	0.67	1.06	0.42	1.61	4
H26N28	0.42	5.5	1.09	1.47	0.10	16
H31N16	0.30	2.5	1.38	2.00	0.32	4
A32S03	0.08	0.83	1.55	0.13	3.15	2
N30S03	0.06	1.87	1.71	0.44	3.67	7

The experiments revealed that, at high compressibility (case H17N28 and below), U_c closely approaches U_1 or U_2, depending on the test case. This is a large deviation from (3) and produces the surprising convective Mach number trends seen on the table. One gets a better view of that discrepancy when the experimental M_{c_1} and M_{c_2} are plotted versus each other. This is done in Fig. 6, where the theoretical values are also included. Dashed lines connect the theoretical and experimental data for each case. The slight deviation of the theoretical points from a perfect diagonal, implied by (2), is due to the small effect of different γ's. The difference between theory and experiment is striking: instead of being equal or close, M_{c_1} and M_{c_2} are very different, one low subsonic and the other sonic or supersonic.

Equally surprising is the fact that the side of the shear layer with the higher M_c is not the same from case to case. In some cases M_{c_1} is higher while in others M_{c_2} is higher. There is no consistency of these trends based on quantities that are frame-of-reference independent, namely on $\frac{\rho_2}{\rho_1}$ and on $\frac{\gamma_2}{\gamma_1}$. For example, cases H31N16 and N30S03 have similar $\frac{\rho_2}{\rho_1}$ and $\frac{\gamma_2}{\gamma_1}$, yet their M_c distributions are different.

However, there is an apparent consistency based on the free stream Mach numbers: in supersonic-supersonic combinations, M_{c_1} is always highest ($U_c \rightarrow U_2$) while in supersonic-subsonic combinations, M_{c_2} is always highest ($U_c \rightarrow U_1$). This baffling trend could be a coincidence or the result of a subtle flow-field change that occurs when the low-speed stream goes from subsonic to supersonic. A possible reason for such change is given in the discussion section.

Revised Structure Model

It is evident that the relationship between M_{c_1} and M_{c_2}, derived from the existing large-scale structure model (Fig. 2), is grossly inaccurate for high compressibility levels. The basis of that model, however, is still believed to be sound: in the convective frame, fluid engulfed into the mixing zone has to come to rest at some point between two structures, and the pressures there must balance for that point to be stable. The assumption of a stationary stagnation point could be debatable. Since the flow is turbulent, the stagnation point could be shifting around, thus adding a time dependence to the equilibrium pressure condition. Judging from the two-spark schlieren photos, however, this effect seems small. For example, in the photo of case H17N28 (Fig. 5) the structure features are remarkably frozen from one exposure to the next, although they are experiencing a shear of 600 m/s.

It is the process by which fluid comes to rest at the stagnation point that needs critical examination. The existing model assumes this process to be isentropic. To make the model more realistic for the compressible case, the dissipative effects of shock waves must be added. A shock wave formed on the structure could cause considerable total-pressure drop along the streamline leading to the stagnation point. If shock waves appear symmetrically on the structure, that loss would be similar on both sides and (2) would still be a good approximation.

There is, however, potential for asymmetric situations. A "cat's eyes" idealization of a large-scale structure sytem, depicted in Fig. 7, helps visualize the following argument. We place ourselves in the convective frame of reference and assume that the two free streams have equal static pressures. In that frame, suppose that the Mach number of the upper free stream, M_{c_1}, is supersonic. As in flow around a cylinder or a thick airfoil, the Mach number near the structure is higher than the free stream Mach number. Flow along the top edge of the structure turns and accelerates through a Prandtl-Meyer expansion fan. As a result, the Mach number ahead of the stagnation

point is substantially higher than M_{c_1}. Flow comes to rest at the stagnation point by means of a normal shock located a short distance upstream of that point. A normal shock at that high Mach number is strong enough that the total pressure downstream of the shock, i.e., the pressure experienced by the stagnation point on that side, is reduced to the level of the *static* pressure in the free streams. As an example, consider a case with M_{c_1}=1.0 and γ_1=1.4. For simplicity, assume that the Mach number at the top of the structure equals M_{c_1}. Suppose that the shock occurs at a flow inclination of 40 deg. with respect to the free stream. From the Prandtl-Meyer function, the Mach number before the shock is found to be 2.4, sufficiently high that the total pressure after the shock equals the free stream static pressure.

In the convective frame again, the free stream Mach number of the lower side, M_{c_2}, must be such that the stagnation point is pressure balanced. Two situtations are now possible· a *symmetric* one, already noted above, in which the lower flow is also supersonic with $M_{c_2} \approx M_{c_1}$, with a similarly-strong shock forming on the lower side of the structure; an *asymmetric* one, in which the lower flow is subsonic ($M_{c_2} \approx 0$), with the resulting total pressure on that side close to the free stream static pressure. Since no shocks are possible at that low Mach number, the total pressure remains virtually constant along the streamline leading to the stagnation point and balances the total pressure produced by the upper side's shock. Hence, the stagnation point is still stable, although M_{c_1} and M_{c_2} are very different. These two situations are illustrated in Fig. 7, where their respective total-pressure distibutions along the stagnation streamline are sketched.

Obviously, the same argument can be considered with M_{c_2} given supersonic, in which case one gets $M_{c_1} \approx M_{c_2}$ (symmetric) or $M_{c_1} \approx 0$ (asymmetric). So a total of three situations are possible, one symmetric and two asymmetric.

It is thus seen that inclusion of shocks in the system can dramatically alter the condition for pressure balance of the stagnation point. Although not proposed as the only possible explanation, the revised model rationalizes the basic experimental trends produced here. In its present form, however, it cannot predict which side of the layer will have the higher M_c. Also, it does not explain why given the symmetric and asymmetric possibilities at high compressibility, the flow here always prefers the asymmetric one.

Significance of $\frac{\Delta U}{a_1+a_2}$

It is important to develop a means of estimating the likelihood of asymmetric situations. According to the revised model, flow along the structure boundary, as seen by the structure, must be supersonic for such situation to be possible. Consequently, the free stream convective Mach number, M_c, must exceed some critical value, M_c^*. As noted earlier, flow in the vicinity of the structure is faster than in the free stream, so M_c^* could be less than 1. A reasonable range for M_c^* is $0.5 < M_c^* < 1$. For an asymmetric situation to be possible, we must then have $M_{c_1} > M_c^*$ or $M_{c_2} > M_c^*$.

The pertinent question to ask is under what conditions will the flow have no choice but to have at least one of the M_c's greater than M_c^*. To help answer that, the diagram of Fig 8 is drawn. It shows the dependence of M_{c_1} and M_{c_2} on U_c from their definitions (2). U_c is bounded by the free stream velocities, U_2 and U_1. The question is now rephrased as follows: regardless of what value U_c takes in the interval $[U_2,U_1]$, what criterion ensures that M_{c_1} or M_{c_2} or both will exceed M_c^*? The answer is obvious from the diagram. The M_{c_1} and M_{c_2} lines form a boundary whose minimum occurs at $M_{c_1} = M_{c_2} = \frac{\Delta U}{a_1+a_2}$. Thus the criterion

$$\frac{\Delta U}{a_1 + a_2} > M_c^* \qquad (4)$$

guarantees that, no matter what the value of U_c is, at least one of the M_c's will exceed M_c^* and that asymmetric solutions will therefore be likely.

It is evident from Fig. 8 that asymmetric solutions are still possible when $\frac{\Delta U}{a_1+a_2} < M_c^*$. In that regime, however, the flow has the choice of a subsonic structure, that is, one with both M_c's less than M_c^* and to which the isentropic model applies. Given the symmetric choice with subsonic flow and the asymmetric choice with a strong shock wave, it is unlikely that the flow will prefer the highly-dissipative asymmetic one.

Judging from the results of this study, a good guess for M_c^* is 0.6. The experimentally-encountered flow states can then be summarized as follows:

$\frac{\Delta U}{a_1+a_2} < 0.6$ Symmetric situations

$\frac{\Delta U}{a_1+a_2} > 0.6$ Asymmetric situations

The parameter $\frac{\Delta U}{a_1+a_2}$, originally a byproduct of the isentropic model, now takes a significance of its own. It defines the possibilities for asymmetric or symmetric states, and does so in a way largely independent of a specific large-scale structure model. It can be considered as a broad measure of shear-flow compressibility, since its value does not depend on shear-layer side.

The actual physics of the mixing, however, depend on the individual convective Mach numbers. In particular, they depend strongly on the higher the two M_c's, denoted $M_{c_{max}}$. The lower M_c is always low subsonic, so its influence is weaker. There is a interesting correlation between $M_{c_{max}}$ and $\frac{\Delta U}{a_1+a_2}$, shown in Fig. 9, where a monotonic trend is observed.

Structure Obliquity

Implicit in the preceding analysis and discussion is the assumption that the spanwise turbulent structure is two-dimensional. It is possible, however, that the structure is oblique, with a direction of propagation inclined at an angle β to the mean flow direction The compressibility of such structure is governed by an effective convective Mach number

$$M_{c_{eff}} = M_c cos\beta \qquad (5)$$

rather than by M_c. For large β, greater than 30 deg., this could bring drastic changes to the flowfield since a structure with $M_c > 1$ may effectively be subsonic. Morkovin[11] proposes that oblique structures begin dominating the flow field once M_c becomes supersonic.

The best way to to visually determine flow three-dimensionality is to obtain a plan view of the shear layer, which necessitates windows on the top and botton walls of the test section. In the current facility, such windows would have been difficult to install. An easier approach, though much inferior, is to visualize the flow in a tilted direction through the existing sidewall windows. This approach was tried and is depicted on Fig. 10. The apparatus was rotated about its flow axis so that the schlieren beam entered the test section at a 12-deg. inclination. Due to the resulting optical distortion, structure obliquity was greatly amplified on the image. For example, a 30-deg. obliquity would have appeared as 70-deg. obliquity on the photos. Therefore, only obliquity that exceeded 70 deg. on the photo could be considered substantial in accordance with (5).

Tilted-view experiments were tried with cases H17N28 and H26N28. The knife edge was oriented perpendicular to the streamwise direction to emphasize gradients in that same direction. Although the pictures suffer from lack of clarity, inherent to the high distortion, features of structures were picked up. By following their evolution through the two-spark system, such features were distinguished from stationary shock waves that would otherwise have created confusion.

The structures do not appear to be convecting in a highly-oblique fashion. Obliquity on the photos did not exceed 45 deg., corresponding to 15-deg. real obliquity. Fig. 11 shows a two-spark photo of case H17N28. The trailing edge is at the left boundary. Arrows indicate a spanwise structure and its later position. That structure looks roughly two-dimensional and is representative of structures seen in other photos of that case and in photos of case H26N28. The convective velocity computed from the photo agrees with that obtained from the untilted experiments (Fig. 5).

It must be emphasized that visualizing the flow with such large optical distortion is not a reliable means of detecting three dimensionality. The results presented in this section should therefore be treated as very preliminary.

Trailing-Edge Devices

Equation (5) indicates that if the flow is made highly three dimensional, its convective Mach numbers would effectively be reduced. From Fig. 2, it is evident that this could cause the growth rate to increase. Several experiments were conducted with the the goal of enhancing three dimensionality, and hence mixing, through trailing-edge modifications. Three types of trailing-edge devices were tried: a vortex generator; trip wires oriented at 60 deg. to the trailing edge; a sawtooth extension of the trailing edge, with teeth inclined at 40 deg. They are shown schematically in Fig. 12 with relevant dimensions.

The devices were applied to case H17N28. The boundary-layer momentum thicknesses immediately upstream of the devices were calculated to be θ_1=0.1mm and θ_2=0.05mm, approximately. On the growth-rate versus M_c curve (Fig. 2), this case is located at the kink where the growth rate bottoms out. Thus a decrease in $M_{c_{eff}}$, even a small one, should

have increased the growth rate by a noticeable amount.

None of the devices enhanced the growth rate by more than 5%. To illustrate the insensitivity of the flow to the mixing-enhancement attempts, Fig. 13 shows a photo of case H17N28 with and without vortex generator. The growth rates appear almost identical. Tilted views of that flow did not appear different from the cases with clean trailing edge.

Strange Waves

As mentioned earlier, schlieren photos with the knife edge perpendicular to the flow direction were also produced in the experiment. This knife-edge orientation picks up gradients in the streamwise direction, which are generally much weaker than those in the transverse direction. It gives a more detailed view of turbulence, since the bias from the refractive-index difference between the two streams is effectively removed. In fact, it shows that the shear layer becomes turbulent immediately downstream of the trailing edge (Fig. 14), something that is hard to establish from pictures taken with a parallel knife edge (Fig. 13). It was mainly applied to cases H17N28 and H26N28.

A peculiar phenomenon was observed when visualizing case H26N28 in that fashion. Waves that were roughly normal to the flow direction and of smooth texture appeared consistently on every photo of that case. Fig. 14 shows a typical one. The waves extend into both free streams and are relatively stationary. They did not appear in case H17N28, perhaps because they did not exist or because they were too weak.

Although these waves cannot yet be fully explained, it is useful to examine what they are not: they are not normal shock waves, or the pressure rise across them would have been enormous; they are not radiating directly from the structure, or a regular pattern with slope equal to the Mach angle at M_{c_1}=1.47 (43 deg.) would have formed. They are not caused by gradients external to the test section, because photos with no flow during the same experiment showed a uniform background.

These waves are thought here to be caused by an intricate interaction between a supersonic structure and the test-section walls and their boundary layers. The fact that they appear in case H26N28 with M_{c_1}=1.47 and they do not appear, or are too weak, in case H17N28 with M_{c_1}=0.83 supports that hypothesis. A structure with M_{c_1}=1.47 emits Mach waves that reach the walls and reflect back on the main flow, creating a complex pressure-wave system. A structure with M_{c_1}=0.83 cannot emit Mach waves except within its close proximity where the Mach number is supersonic.

If the waves are indeed generated in this manner, it is still unclear why they do not convect with the structure but remain almost stationary. It is possible that they are initially created by a mechanism similar to the one described above, but then acquire a nature of their own. Obviously, more experiments are needed to explain this strange phenomenon.

Discussion

The experimental results raise the question as to what the appropriate compressibility-effect parameter for the shear layer is. Previously, the isentropic model with $M_{c_1} \approx M_{c_2}$ made the answer easy: either M_c was a suitable choice. Now that that model is found to be inaccurate, that choice must be reexamined. The results of this study suggest two ways to describe shear-flow compressibility in a consistent manner. One way is to use $M_{c_{max}}$, the larger of the two M_c's. Since the lower M_c is found here to be always low subsonic, its contribution is secondary. Thus, $M_{c_{max}}$ directly defines the compressibility associated with the large-scale structure. An estimate for $M_{c_{max}}$ can be obtained from Fig. 8, assuming that the curve has universal character. That leads to the other, more indirect, way of describing compressibility by the parameter $\frac{\Delta U}{a_1+a_2}$. As already noted, it determines when a structure *has* to be supersonic regardless of the value of U_c. Its good correlation with $M_{c_{max}}$ suggests that it too is a consistent measure of compressibility. A plot of growth rate versus $\frac{\Delta U}{a_1+a_2}$ would be virtually indistinguishable from the plot of Fig. 2. Plotted versus $M_{c_{max}}$, the growth rate would still fall on a universal curve, provided that the relation of Fig. 8 is itself universal.

The two-spark schlieren photos revealed some remarkable features of the compressible shear layer. Generally, the large-scale structure appears frozen from one exposure to the next, even though the velocity difference across the structure is of the order of the convective velocity and the structure has typically travelled two of its body lengths. There is no evidence of pairing or coalescence. It is thus of great interest to inquire where these structures are "born". If they are generated near the trailing edge, and then

merely convected and expanded downstream, the flow field in the vicinity of the trailing edge, which includes the wake region, may influence their behavior. The difference between supersonic-supersonic and supersonic-subsonic combinations, noted above, could be connected to the fact that the wake zone is more dominant in the former cases than in the latter ones.

Although the revised structure model makes use of shock waves emanating from the structures, such waves are not clearly seen in the schlieren photos. This may be due to the rapid weakening of their strength and their transformation to weak waves by action of the surrounding expansion waves (Fig. 7). In fact, if the shock waves retained their strength far from the structure, they would greatly alter the free stream conditions: U_1 would have to be continuously decreasing and U_2 continuously increasing, leading to an impossible situation for a shear layer. In the experiment, U_1, U_2, and U_c were fairly independent of streamwise location. From that point of view, it is not surprising that such shock waves do not extend far into the free stream.

The asymmetric trends observed in the experiments could have a significant impact on mixing and combustion. The mass entrainment ratio

$$E = \frac{\rho_2}{\rho_1}\,\frac{U_c - U_2}{U_1 - U_c} = \sqrt{\frac{\rho_2\,\gamma_2}{\rho_1\,\gamma_1}}\,\frac{M_{c_2}}{M_{c_1}}$$

is far from unity in the highly-compressible cases due to the large difference between M_{c_1} and M_{c_2}. The uncertainty in predicting which way the asymmetry will occur, hence which side will be preferentially entrained, may pose challenges for the design of efficient supersonic combustors.

These asymmetries are not without theoretical precedent. Similar trends are found in the inviscid linearized stability analysis for an unbounded shear layer with uniform density by Blumen *et al.*[12]: as the convective Mach number exceeds 1, the disturbance phase velocity departs from the mean velocity and approaches either U_1 or U_2. Presence of solid boundaries in the flow can introduce new modes of instability, some of which are asymmetric. Such modes are evident in Tam and Hu's [13] eigenfunction distributions for a bounded shear layer.

Given the radiative nature of a supersonic disturbance, the effects of the surrounding walls cannot be neglected, as is frequently done in the subsonic case. The strange waves seen in the schlieren photos of Fig. 14 are perhaps a hint that walls have to be an integral part of any realistic compressible shear layer model.

The failure of mixing enhancement through efforts to increase flow three-dimensionality may have two different and highly-speculative interpretations: (a) the flow instability is basically two-dimensional and resists any departure from that state; (b) the instability is highly three-dimensional to begin with, in which case the devices would have little to contribute. The visualization of distinct large-scale structures through the schlieren system, which gives a spanwise-integrated view of the flow, and, to a lesser extent, the tilted-view experiments, tend to support argument (a). However, this issue cannot be settled until a direct plan view of the compressible turbulent shear layer is obtained. It must also be noted that this study has by no means exhausted all the methods for efficient mixing enhancement. Other configurations may hold more promise.

Conclusion

Inclusion of shock waves in the model for a compressible large-scale structure gives rise to highly-asymmetric solutions for the convective Mach numbers. This helps interpret the large difference between M_{c_1} and M_{c_2} seen in the experiments. The parameter $\frac{\Delta U}{a_1+a_2}$ delineates the likelihood of asymmetric solutions and is a broad measure of shear-flow compressibility. Tilted-view experiments, although of preliminary nature, did not reveal pronounced obliquity of the large-scale structure. The failure of mixing-enhancement attempts through trailing-edge devices underlines the inherent stability of highly-compressible shear layers.

Acknowledgements

I am indebted to Prof. Anatol Roshko for his advice and support. I am also grateful to Prof. Donald Coles for urging the addition of shock waves to the isentropic model, even before the present experimental results were obtained. This work was sponsored by a grant from the Rockwell International Foundation Tust and by Contract N00014-85-K-0646 of the Office of Naval Research.

References

[1] Papamoschou, D. and Roshko, A., "Observations of Supersonic Free Shear Layers," AIAA Paper 86-0162, Jan. 1986.

[2] Papamoschou, D. and Roshko, A., "The Compressible Turbulent Shear Layer: An Experimental Study," *Journal of Fluid Mechanics*, Vol. 197, Dec. 1988, pp. 453-477.

[3] Flügel, G., "The Design of Jet Pumps," NACA TM 982, July 1941.

[4] Brown, G.L., "The Entrainment and Large Structure in Turbulent Mixing Layers," *Fifth Australasian Conference on Hydraulics and Fluid Mechanics*, Christchurch, New Zealand, 1974, pp. 352-359.

[5] Coles, D., "Prospects for Useful Research on Coherent Structure in the Turbulent Shear Flow," *Proceedings of the Indian Academy of Sciences* , Vol. 4, No. 2, 1981, pp. 111-127.

[6] Dimotakis, P.E., "Two-Dimensional Shear-Layer Entrainment," *AIAA Journal*, Vol. 24, No. 11, pp. 1791-1796.

[7] Bogdanoff, D.W., "Compressibility Effects in Turbulent Shear Layers," *AIAA Journal*, Vol. 21, No. 6, 1983, pp. 926-927.

[8] Brown, G.L. and Roshko, A., "On Density Effects and Large-Scale Structures in Turbulent Mixing Layers," *Journal of Fluid Mechanics*, Vol. 64, No. 4, 1974, pp.775-781.

[9] Papamoschou, D., "Experimental Investigation of Heterogenous Compressible Shear Layers," Ph.D. Thesis, California Institute of Technology, 1986.

[10] Papamoschou, D., "A Two-Spark Schlieren System for Very-High Velocity Measurement," to appear in *Experiments in Fluids*.

[11] Morkovin, M.V., "Transition at Hypersonic Speeds," NASA-CR-178315, ICASE Interim Rep. 1.

[12] Blumen, W., Drazin, D.G., and Billings, D.F., "Shear Layer Instability of an Inviscid Compressible Fluid, No. 2," *Journal of Fluid Mechanics*, Vol. 71, No. 2, 1975, pp. 305-316.

[13] Tam, C.K.W. and Hu, F.Q., "Instabilities of Supersonic Mixing Layers Inside a Rectangular Channel," AIAA Paper 88-3675, July 1988.

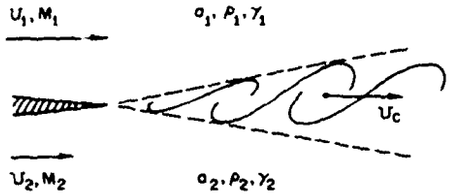

Fig. 1 Shear-layer geometry and nonmenclature.

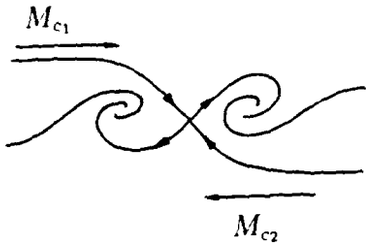

Fig. 2 Isentropic model of large-scale structure.

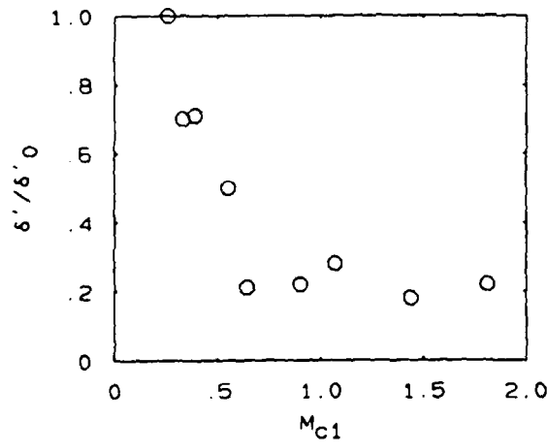

Fig. 3 Normalized growth rate versus theoretical M_{c_1} (Refs 2,9).

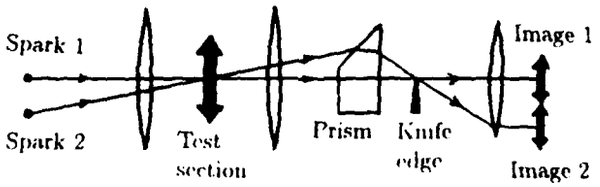

Fig. 4 Operating principle of two-spark schlieren system.

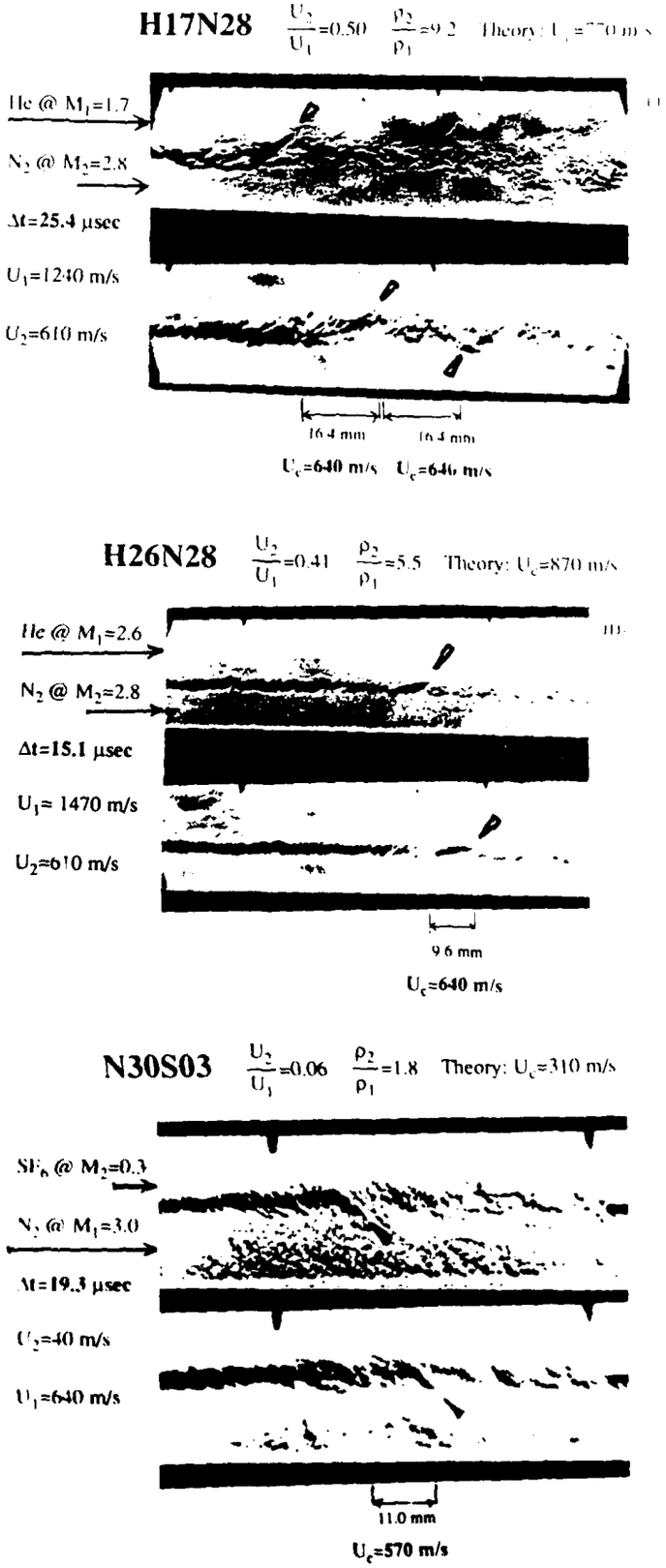

Fig. 5 Two-spark schlieren photos, covering flow from 50mm to 140mm downstream of trailing edge.

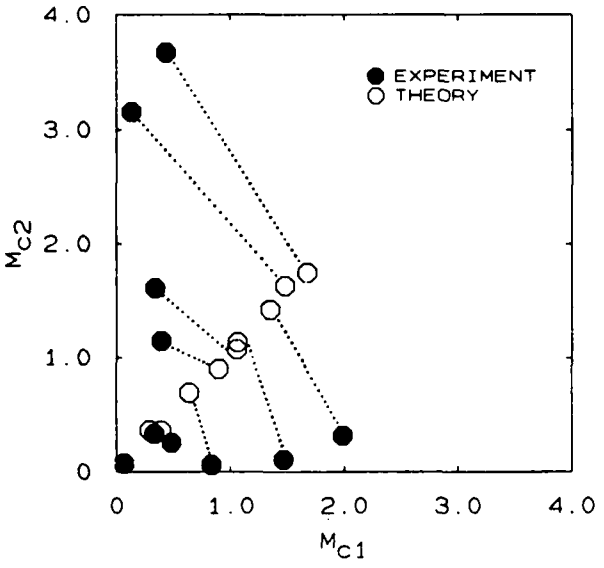

Fig. 6 Experimental and theoretical $M_{c_1} - vs. - M_{c_2}$ plot for the ten cases investigated here.

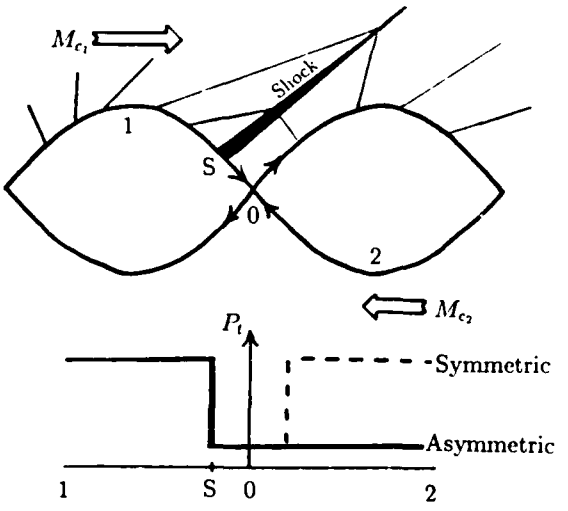

Fig. 7 Revised compressible large-scale-structure model. Sketch of total-pressure distribution (P_t) along streamlines leading to stagnation point (0) illustrates the symmetric and asymmetric possibilities.

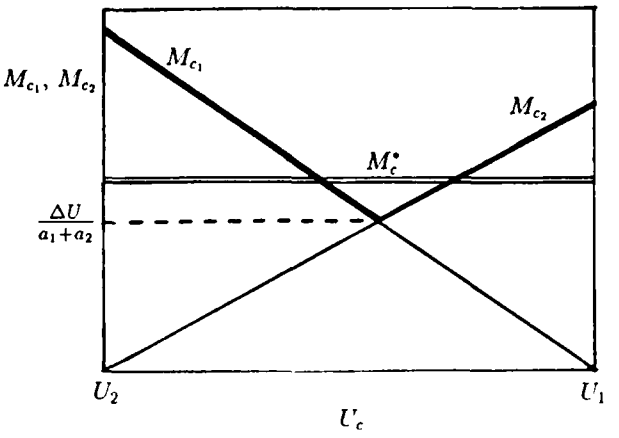

Fig. 8 Dependence of M_{c_1} and M_{c_2} on U_c for arbitrary conditions. M_c^* indicates the level to be exceeded for asymmetric situations to be likely.

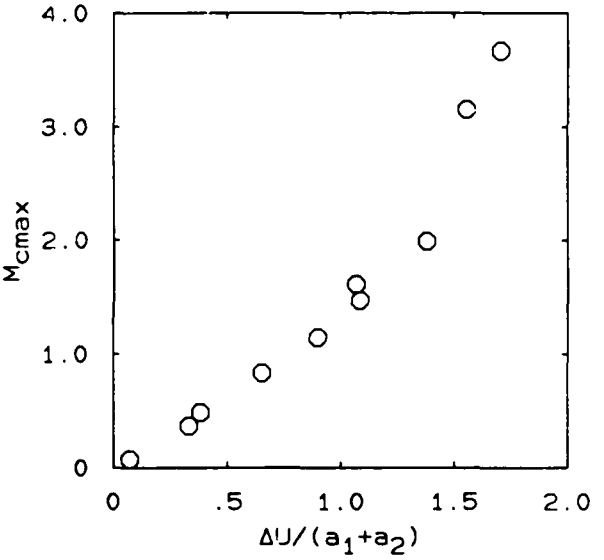

Fig. 9 The maximum of experimental M_{c_1} and M_{c_2}, $M_{c_{max}}$, versus $\frac{\Delta U}{a_1+a_2}$.

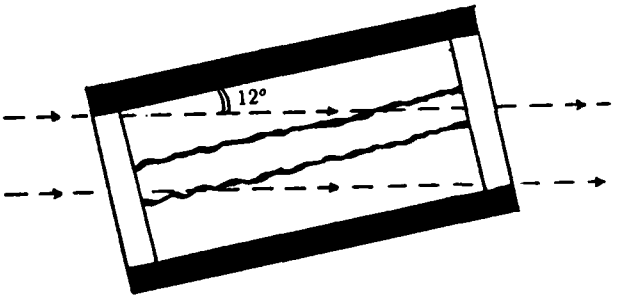

Fig. 10 Tilted-view method for visualizing spanwise structure. Flow is coming out of the paper.

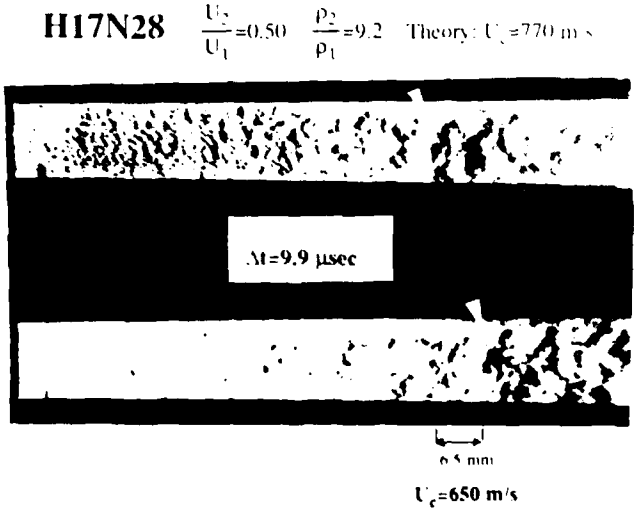

Fig. 11 Tilted view of case H17N28 with U_c measurement.

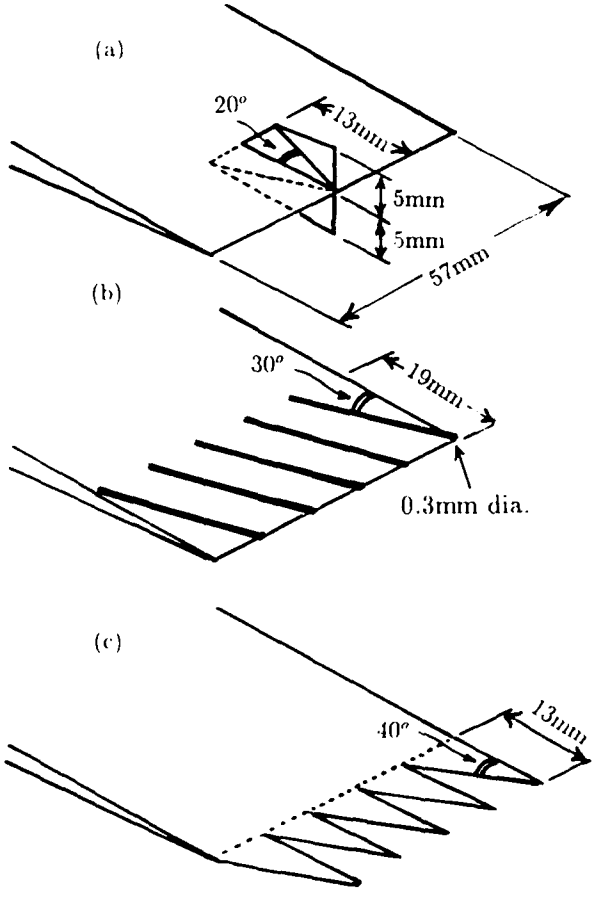

Fig. 12 Trailing-edge modifications: (a) vortex generator; (b) slanted trip wires; (c) saw-tooth extension.

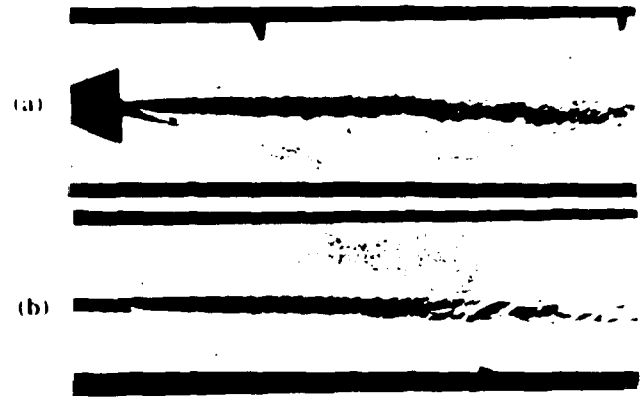

Fig. 13 Near-field (0 to 90mm) photo of case H17N28: (a) with vortex generator; (b) without.

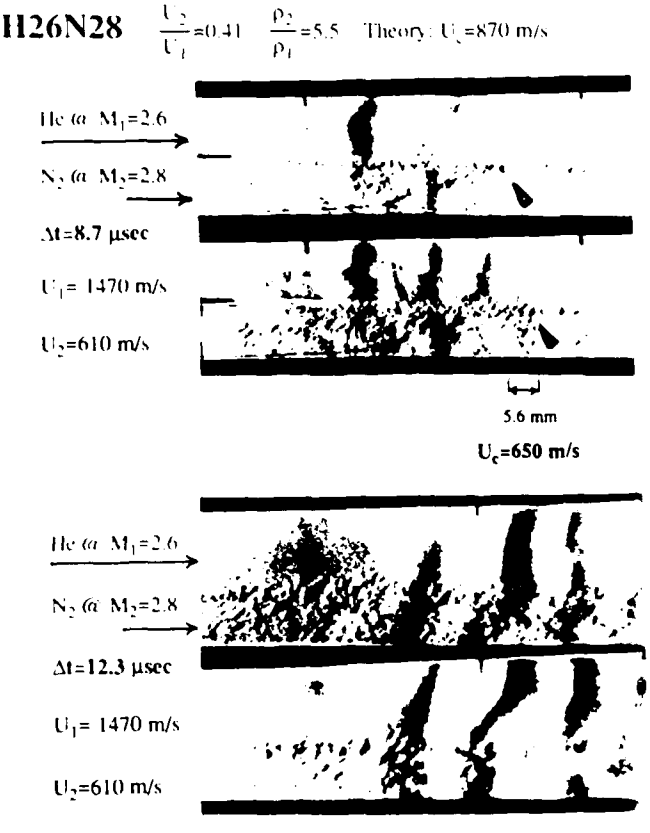

Fig. 14 Two-spark photos of case H26N28 taken with knife edge vertical. Upper photo covers near field (0 to 90mm), where U_c measurement is shown; lower photo covers far field (50mm to 140mm). Strange waves are visible in both photos.